Supplemental text for "High pressure metal–silicate partitioning of Ni, Co, V, Cr, Si, and O" by R.A. Fischer, Y. Nakajima, A.J. Campbell, D.J. Frost, D. Harries, F. Langenhorst, N. Miyajima, K. Pollok, and D.C. Rubie

Detection limits and uncertainties in EDX analyses:

To verify that our EDX analyses were above detection limits (*DL*), we ensured that the background-subtracted peak intensities are greater than three times the standard deviation (1σ) of the counts in the background under the peak. For an alloy of elements *A* and *B*, this can be expressed as:

$$C_B(DL) = \frac{3\sqrt{2I_B^b}}{I_A - I_A^b} \times k(B/A) \times C_A$$

where C_B and C_A are the concentrations of elements *B* and *A* in wt%, I_B^b and I_A^b are background intensities of elements *B* and *A*, I_A is the raw integrated peak intensity of element *A*, and $k(B/A)$ is the Cliff-Lorimer k-factor.

Sample R139 was recovered from 56 GPa and 4360 K, and we report that the silicate melt contains 300 ppm CrO. An example of one of our EDX spectra on the silicate melt in this sample is shown below, obtained with a collection time of ~600 seconds.

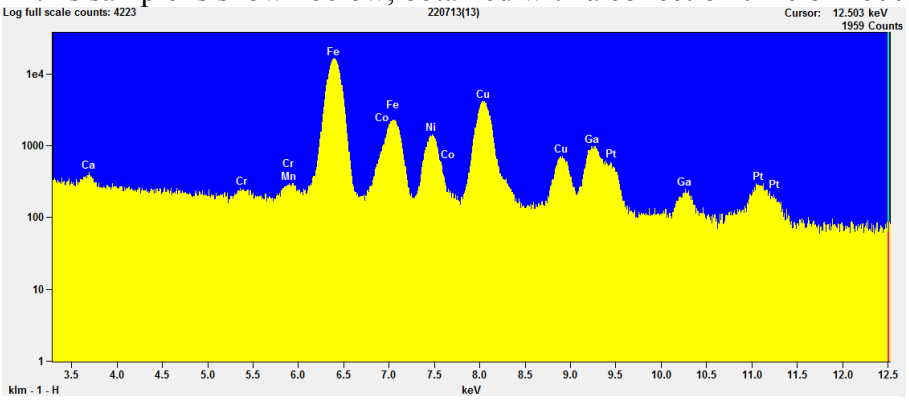

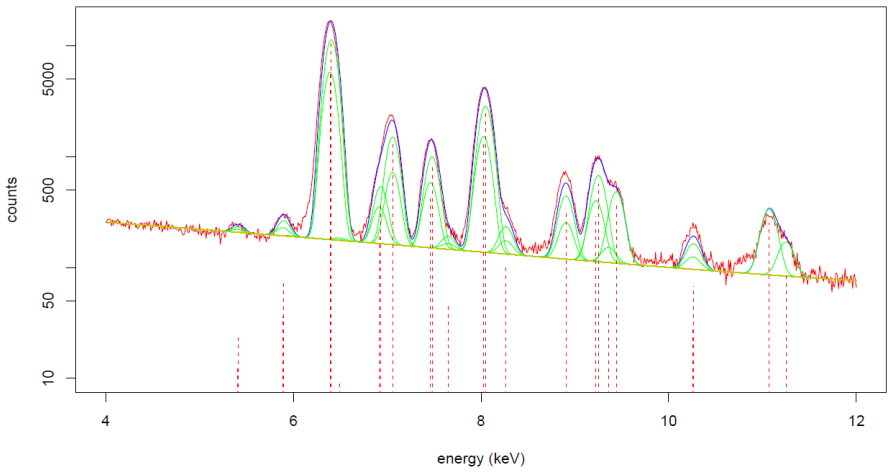

Sample R142 was recovered from 57 GPa and 4440 K, and we report that the metallic melt contains 840 ppm V. An example of one of our EDX spectra on the metallic melt in this sample is shown below, obtained with a collection time of ~600 seconds.

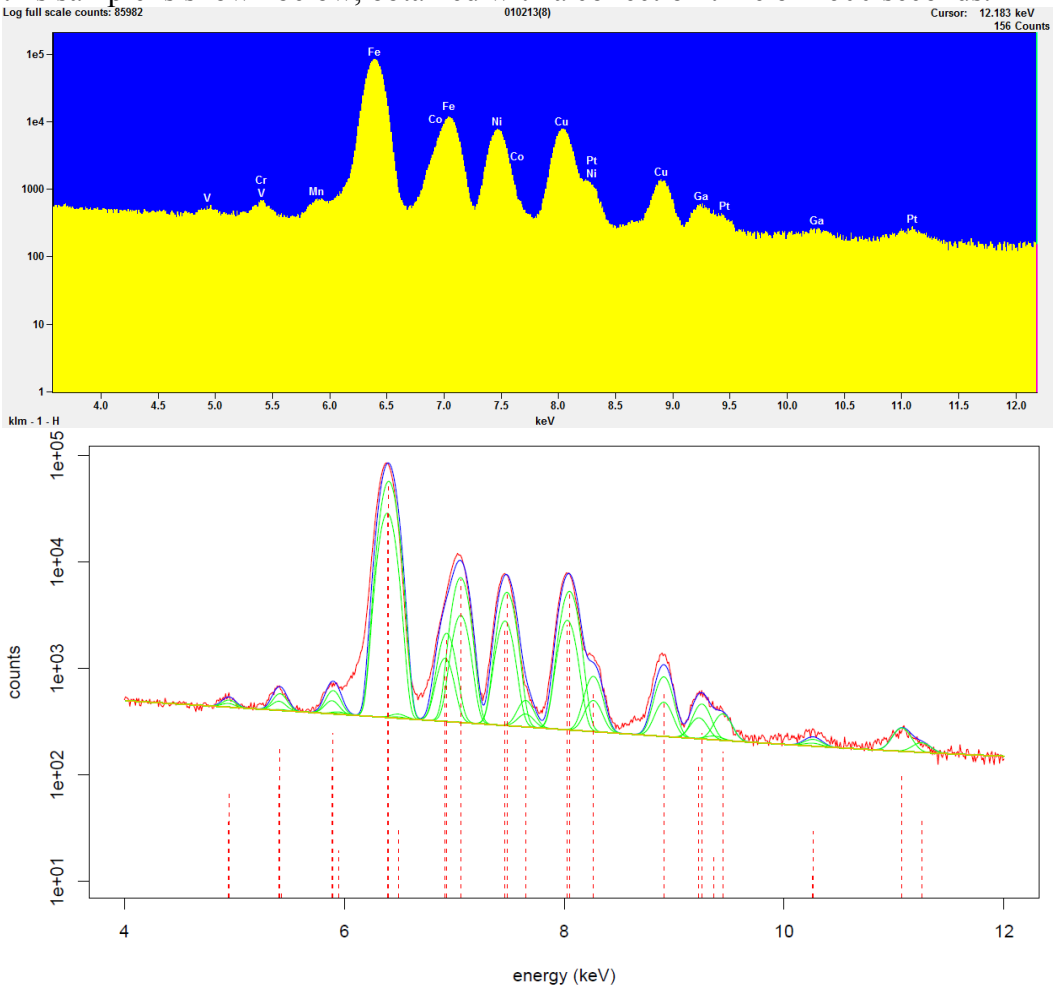

We calculated the detection limits by summing up the counts within a window ~140 eV wide (FWHM) and centered on the peak. For CrO in the silicate melt of R139, we find a detection limit of 250 ppm. For V in the metallic melt of R142, we find a detection limit of 240 ppm. Therefore, the detected peaks are statistically significant.

Analytical uncertainties of Cr, V, Ni, and Co in EDX measurements are based on uncertainties in the number of counts in the spectra and uncertainties in the k-factors that we used. Typically these analytical uncertainties are significantly smaller than a standard deviation of multiple measurements, so in most cases we report uncertainties as a standard deviation. However, in the case of V and Cr in the metal of our three highest pressure samples, the analytical uncertainty represented a significant contribution to the total uncertainty and was used in the calculation.

Evaluation of TEM-EDX spectra involved the use of experimentally-calibrated k-factors of oxygen, magnesium, silicon, calcium, chromium, and iron (van Cappellen, 1990), k-factors estimated from theory for vanadium, manganese, cobalt, and nickel, and an

absorption correction based on approximate densities (3.9 g/cm^3 for the quenched silicate melt and 8 g/cm^3 for the quenched metallic melt) and the sample thicknesses (e.g., 60–150 nm) in the measured areas. For example, if the theoretical k-factor (Fe/Si) is 0.9017 and our experimentally-calibrated k-factor is 1.462, based on a natural pyrope–almandine garnet standard, we corrected all theoretical k-factors by a factor of 1.462/0.9017. The list of k-factors that we used is below.

Element	**M/Si**	**M/Fe**	**Source**
Mg	0.92	0.629	Calibrated
Ca	1.226	0.839	Calibrated
V	1.371	0.938	Theoretical
Cr	1.418	0.970	Calibrated
Mn	1.447	0.990	Theoretical
Fe	1.462	1.000	Calibrated
Co	1.55	1.060	Theoretical
Ni	1.568	1.073	Theoretical

We cross-checked the detection limit and accuracy in EDX measurements of San Carlos olivine, obtained under the same conditions (acquisition time of ~600 seconds, count rate of ~5.5 kcps).

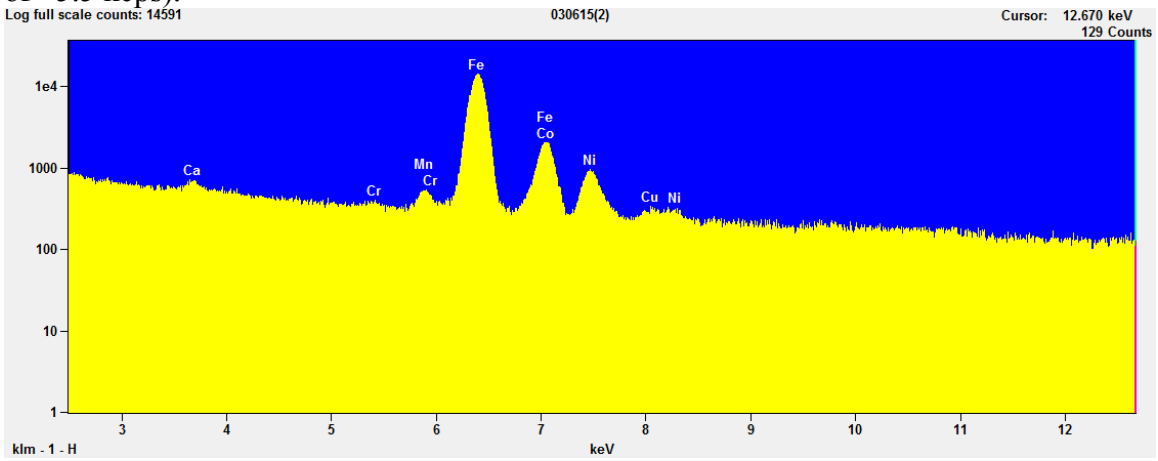

(in log scale)

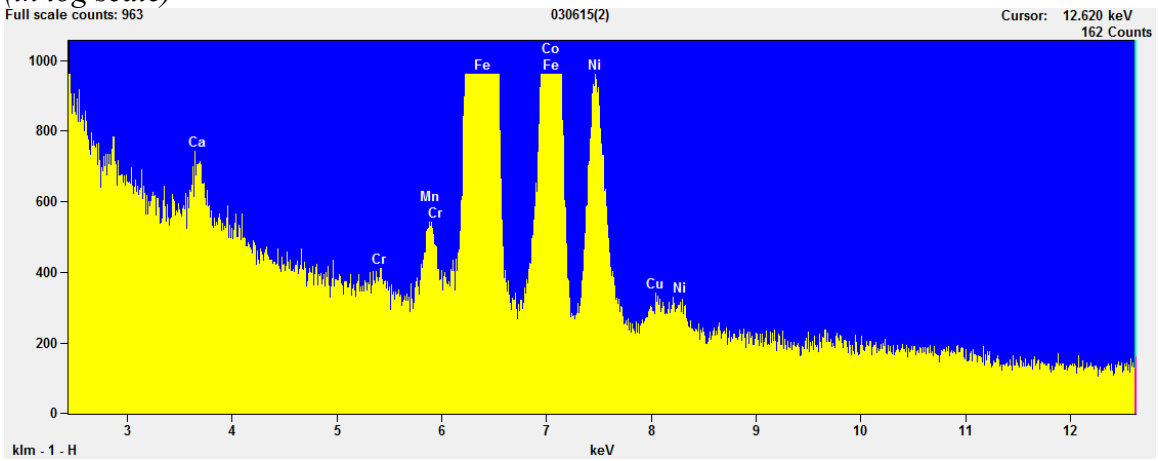

(in linear scale)

Trace element abundances in the olivine are compared to those reported by Spandler and O'Neill (2010). We find 3530 ppm Ni, 500 ppm Ca, and 170 ppm Cr, illustrating that our EDX quantitative analysis results of these elements are in reasonable agreement with those of Spandler and O'Neill (2010).

References:

Spandler C. and O'Neill H. St.C. (2010) Diffusion and partition coefficients of minor and trace elements in San Carlos olivine at 1,300°C with some geochemical implications. *Contrib. Mineral. Petrol.* **159**, 791–818.

van Cappellen E. (1990) The parameterless correction method in X-ray microanalysis. *Microsc. Microanal. Microstruct.* **1**, 1–22.

Appendix Figure Captions

Figure A.1: Residuals on the fits to Ni (a) and Co (b). Only data from the present study (triangles) have error bars, showing the uncertainty on the measurements. Data from $P > 25$ GPa are color-coded by pressure (purple: 25–50 GPa, blue: 50–75 GPa, green: 75–100 GPa) with the symbol indicating the study. Data from 5–25 GPa are taken from Bouhifd and Jephcoat (2003), Bouhifd et al. (2013), Chabot et al. (2005), Corgne et al. (2008), Geßmann and Rubie (1998), Hillgren et al. (1996), Jana and Walker (1997), Kegler et al. (2008), Siebert et al. (2011), Thibault and Walter (1995), and this study. Corresponding data are shown in Fig. 4.

Figure A.2: Exchange coefficient of Ni (a) and Co (b) as a function of pressure, color-coded by temperature range. Lines are isotherms calculated from the fits in Table 2 for the midpoint of the temperature range indicated. Data are from Bouhifd and Jephcoat (2003, 2011), Bouhifd et al. (2013), Chabot et al. (2005), Corgne et al. (2008), Geßmann and Rubie (1998), Hillgren et al. (1996), Jana and Walker (1997), Kegler et al. (2008), Siebert et al. (2011, 2012), Thibault and Walter (1995), and this study.

Figure A.3: Exchange coefficient of Ni from various studies. Lines are isobars calculated to show the temperature dependence of partitioning at a fixed pressure. Solid lines: results from this study (also shown in Fig. 4 of the main text). Dashed lines: Siebert et al. (2012). Dotted lines: Campbell et al. (2009), calculated from the Fe–FeO and Ni–NiO oxygen fugacity buffers, assuming ideality. All lines are color-coded according to the legend. All three studies show a reversal in the trend of siderophility versus temperature at ~45 GPa.

Figure A.4: Residuals on the fits to Si (a) and O (b). Only data from the present study (triangles) have error bars, showing the uncertainty on the measurements. Data from $P > 25$ GPa are color-coded by pressure (purple: 25–50 GPa, blue: 50–75 GPa, green: 75–100 GPa) with the symbol indicating the study. Data from 5–25 GPa are taken from Chabot et al. (2005), Corgne et al. (2008), Geßmann and Rubie (1998), Hillgren et al. (1996), Ito et al. (1995), Jana and Walker (1997), Mann et al. (2009), Ricolleau et al. (2011), Tsuno et al. (2013), and this study. Corresponding data are shown in Fig. 6.

Figure A.5: Residuals on the fits to V (a) and Cr (b). Only data from the present study (triangles) have error bars, showing the uncertainty on the measurements. Data from $P > 25$ GPa are color-coded by pressure (purple: 25–50 GPa, blue: 50–75 GPa, green: 75–100 GPa) with the symbol indicating the study. Data from 5–25 GPa are taken from Corgne et al. (2008), Geßmann and Rubie (1998), Mann et al. (2009), Siebert et al. (2011), Thibault and Walter (1995), Wade and Wood (2005), and this study. Corresponding data are shown in Fig. 5.

Figure A.6: Exchange coefficients of Si (a) and O (b). Uncorrected data (symbols) are shown compared to the fits of Equation 3 (Table 3) corrected to infinitely dilute light elements (lines). Partitioning of Si has no resolvable pressure dependence. The inset in (a) shows the data corrected for no O and C, with Si at infinite dilution; the inset in (b) shows the data corrected for no Si and C, with O at infinite dilution. Only data from the present study (triangles) have error bars. Data from $P > 25$ GPa are color-coded by pressure range (purple: 25–50 GPa, blue: 50–75 GPa, green: 75–100 GPa) with the symbol indicating the study. Data from 5–25 GPa are taken from Chabot et al. (2005), Corgne et al. (2008), Geßmann and Rubie (1998), Hillgren et al.

(1996), Ito et al. (1995), Jana and Walker (1997), Mann et al. (2009), Ricolleau et al. (2011), Tsuno et al. (2013), and this study. Only data without sulfur in the system are shown.

Appendix Table Captions

Table A.1: Starting compositions (in mole fractions) of the two metals used in the diamond anvil cell experiments. Compositions were determined by scanning electron microscopy, with uncertainties reported as the standard deviation of *n* measurements. Values with asterisks (*) are below detection limit within measurement uncertainty.

Table A.2: Conditions, starting materials, and resulting compositions of diamond anvil cell (DAC) experiments and multianvil press (MAP) experiments. Oxygen fugacity is calculated assuming ideality. Starting metal compositions in diamond cell experiments are reported in Table A.1. Starting silicates are olivine unless otherwise indicated. Diamond cell experiment compositions were determined from 4–8 TEM-EDX and EELS analyses, while multianvil press experiment compositions were determined by electron microprobe. All compositions are reported in terms of weight percent. Uncertainties are calculated as standard deviations of multiple measurements, which capture the dominant sources of uncertainty (analytical and k-factor uncertainties were applied to Cr and V concentrations in the metal of three samples).

Table A.3: Pressures, temperatures, compositions, and exchange coefficients from previous experiments. All compositions are in mole fractions. Exchange coefficients have been recalculated to ensure a common definition. Data are taken from Bouhifd and Jephcoat (2003,

2011), Bouhifd et al. (2013), Chabot and Agee (2003), Chabot et al. (2005), Corgne et al. (2008), Geßmann and Rubie (1998), Hillgren et al. (1996), Ito et al. (1995), Jana and Walker (1997), Kegler et al. (2008), Mann et al. (2009), Ricolleau et al. (2011), Righter et al. (2010), Siebert et al. (2011, 2012, 2013), Thibault and Walter (1995), Tsuno et al. (2013), Wade and Wood (2005), and this study. Values with asterisks (*) are outlying data points, which were excluded from the fits on the basis of low measured abundances.

Table A.4: Epsilon interaction parameters found in this study compared to those of several previous studies. All values are calculated at 1873 K. Epsilons from this study are calculated from e_k^i values listed in Table 3.

Table A.5: Variance-covariance matrix describing the fit of Equation 2 to Ni partitioning data. Entries on the diagonal indicate the variance on each fitted parameter, while off-diagonal entries describe the covariance between the two parameters whose row and column intersect there. Matrix is symmetric by definition.

Table A.6: Analogous to Table A.5 for Co.

Table A.7: Analogous to Table A.5 for Si.

Table A.8: Analogous to Table A.5 for O.

Table A.9: Variance-covariance matrix describing the fit of Equation 3 to V partitioning data.

Table A.10: Analogous to Table A.9 for Cr.

Table A.11: Compositions (in weight percent) of the initial bodies in our core formation modeling.

Figure A.1

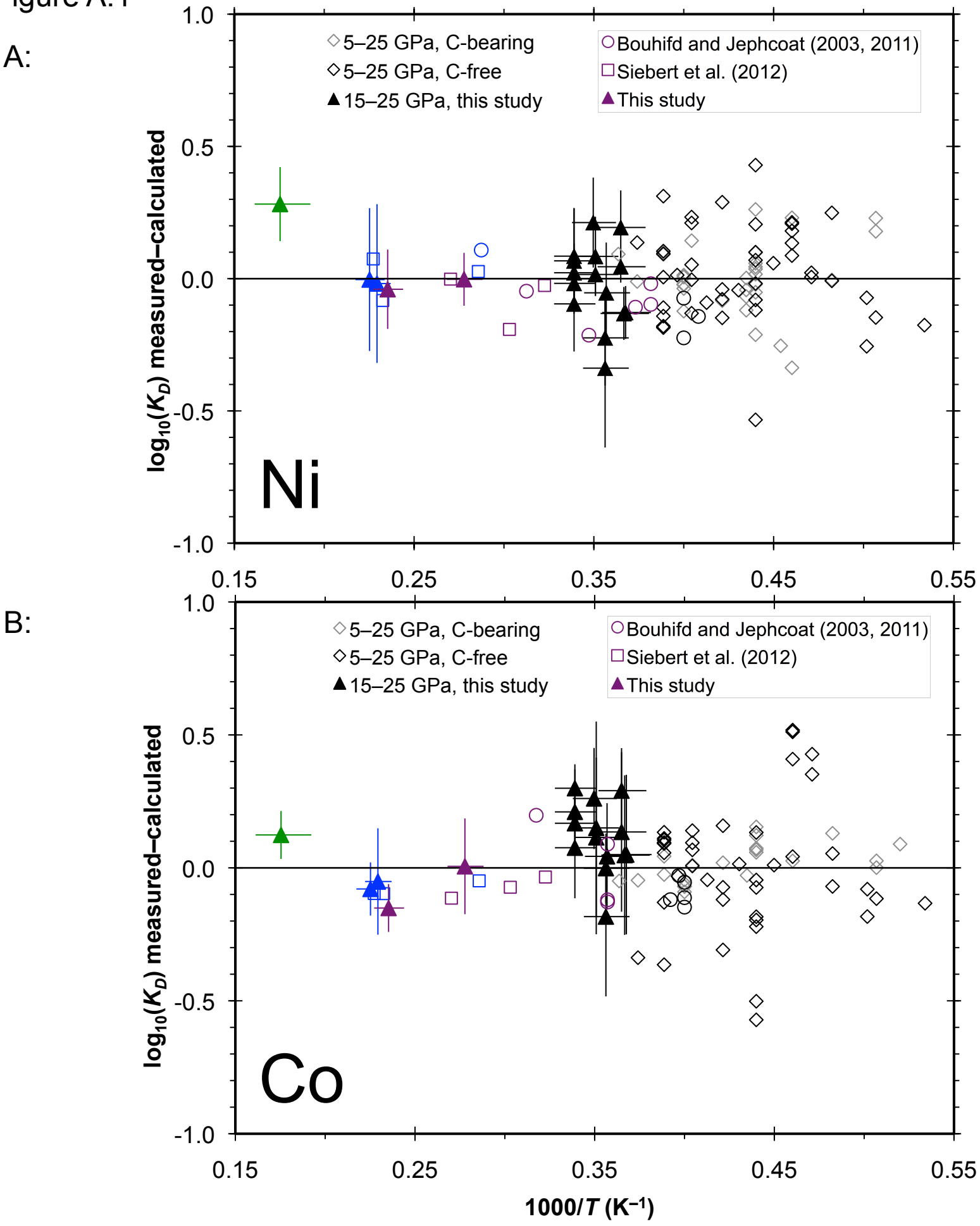
A:
5–25 GPa, C-bearing
5–25 GPa, C-free
15–25 GPa, this study
Bouhifd and Jephcoat (2003, 2011)
Siebert et al. (2012)
This study
Ni
log10(KD) measured–calculated
1.0
0.5
0.0
-0.5
-1.0
0.15
0.25
0.35
0.45
0.55
B:
5–25 GPa, C-bearing
5–25 GPa, C-free
15–25 GPa, this study
Bouhifd and Jephcoat (2003, 2011)
Siebert et al. (2012)
This study
Co
log10(KD) measured–calculated
1000/T (K−1)

Figure A.2

A:

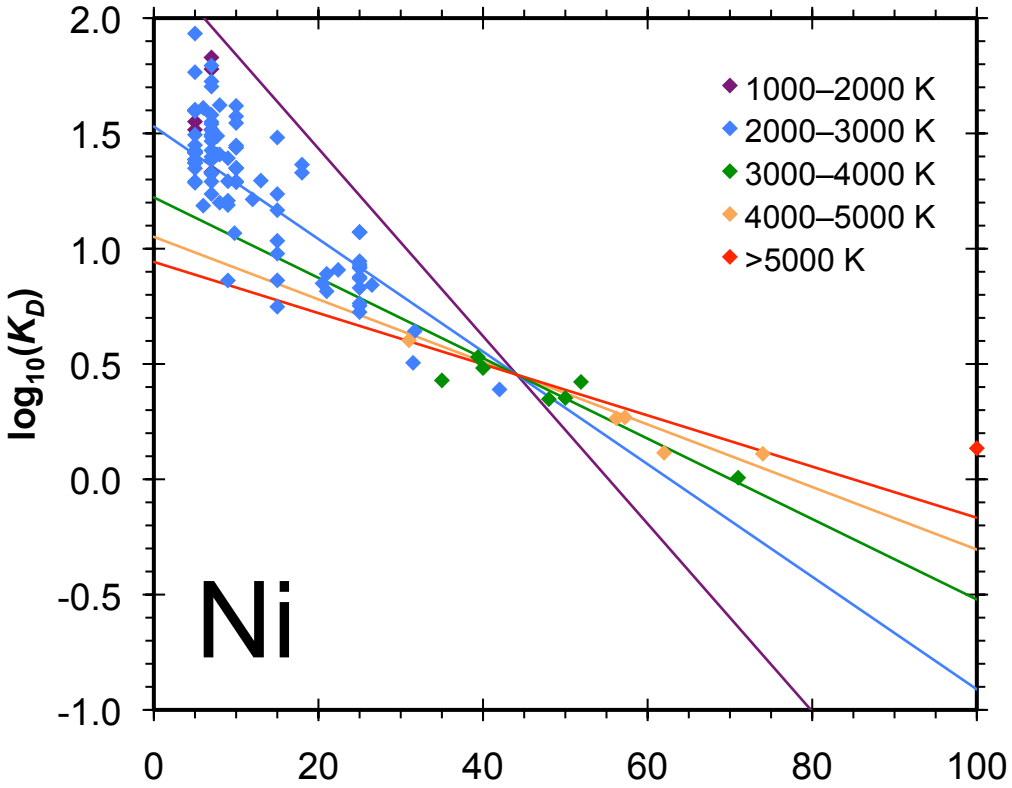
2.0
1.5
1.0
0.5
0.0
-0.5
-1.0
0
20
40
60
80
100
log10(KD)
1000–2000 K
2000–3000 K
3000–4000 K
4000–5000 K
>5000 K
Ni

B:

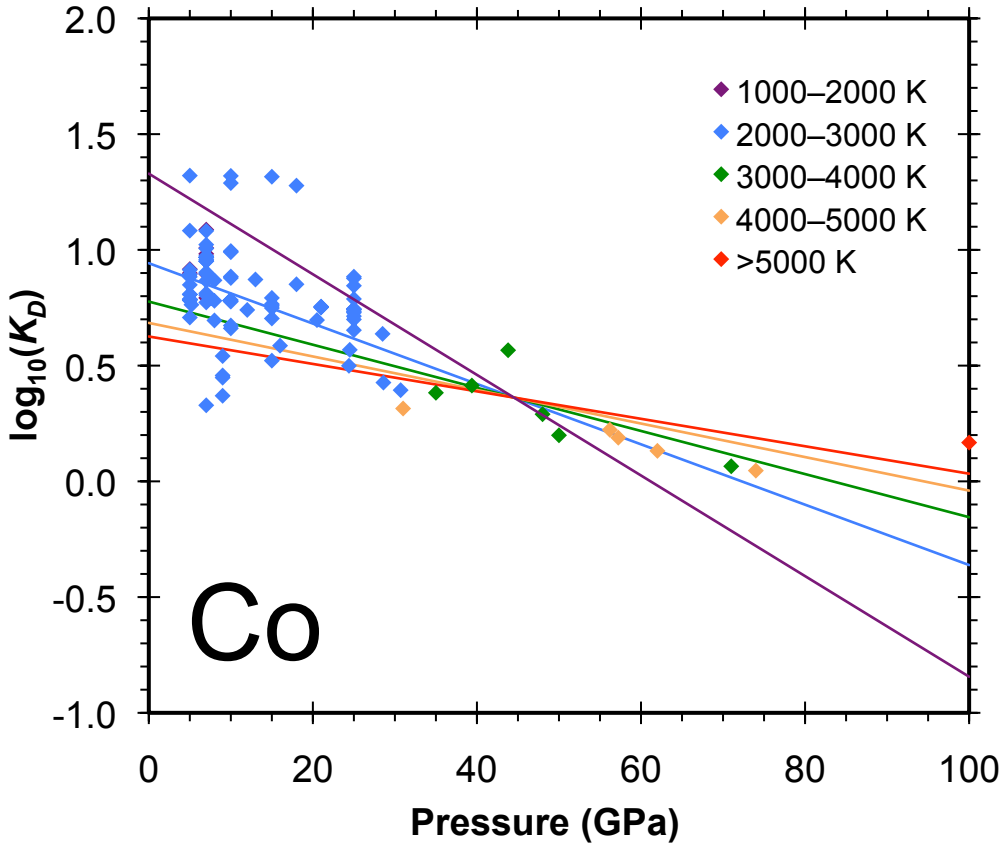
2.0
1.5
1.0
0.5
0.0
-0.5
-1.0
0
20
40
60
80
100
log10(KD)
1000–2000 K
2000–3000 K
3000–4000 K
4000–5000 K
>5000 K
Co
Pressure (GPa)

Figure A.3

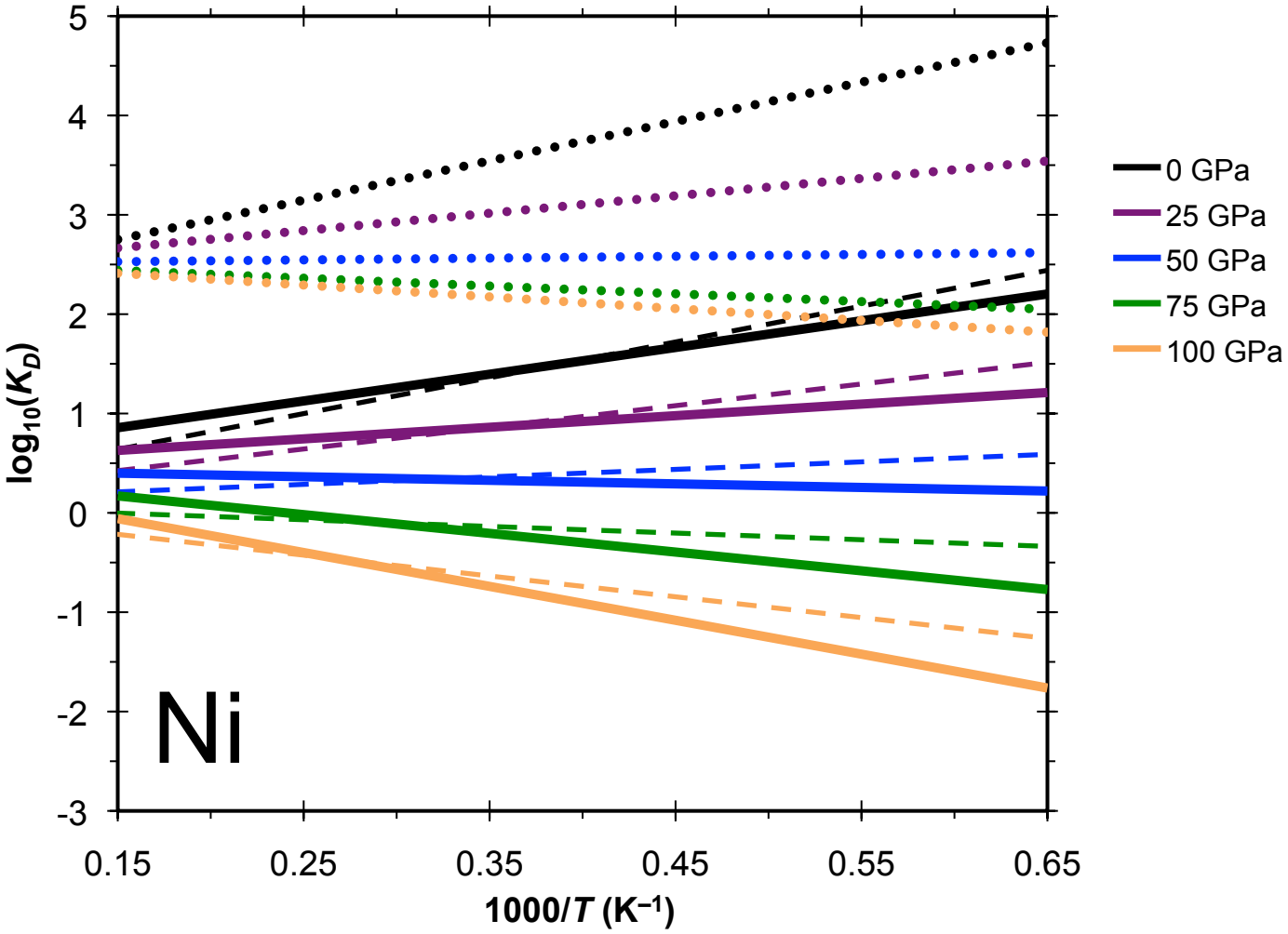
5
4
3
2
1
0
-1
-2
-3
0.15
0.25
0.35
0.45
0.55
0.65
log10(KD)
1000/T (K−1)
Ni
0 GPa
25 GPa
50 GPa
75 GPa
100 GPa

Figure A.4

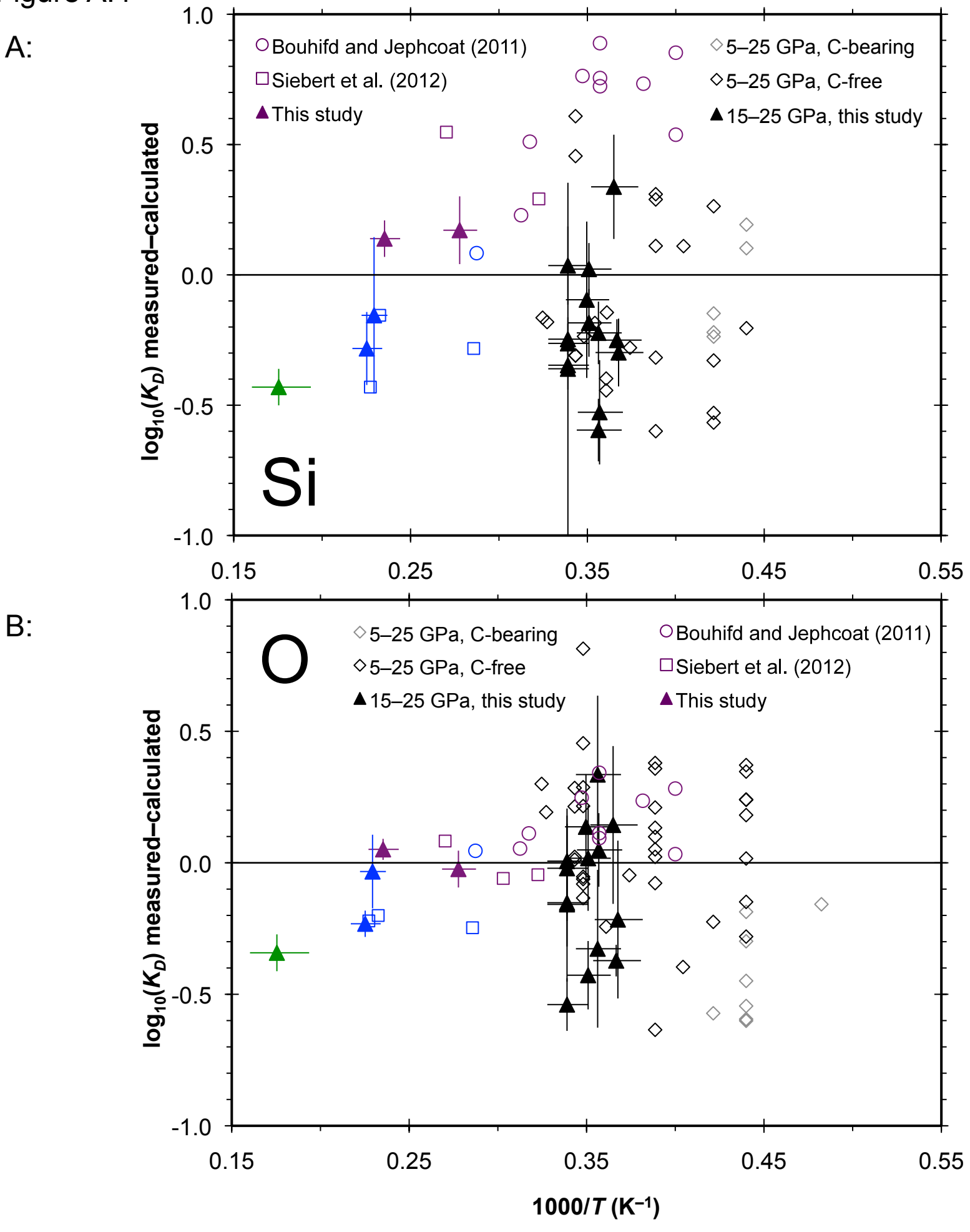
A:
Bouhifd and Jephcoat (2011)
Siebert et al. (2012)
This study
5–25 GPa, C-bearing
5–25 GPa, C-free
15–25 GPa, this study
Si
log10(KD) measured–calculated
1.0
0.5
0.0
-0.5
-1.0
0.15
0.25
0.35
0.45
0.55
B:
O
5–25 GPa, C-bearing
5–25 GPa, C-free
15–25 GPa, this study
Bouhifd and Jephcoat (2011)
Siebert et al. (2012)
This study
log10(KD) measured–calculated
1000/T (K−1)

Figure A.5

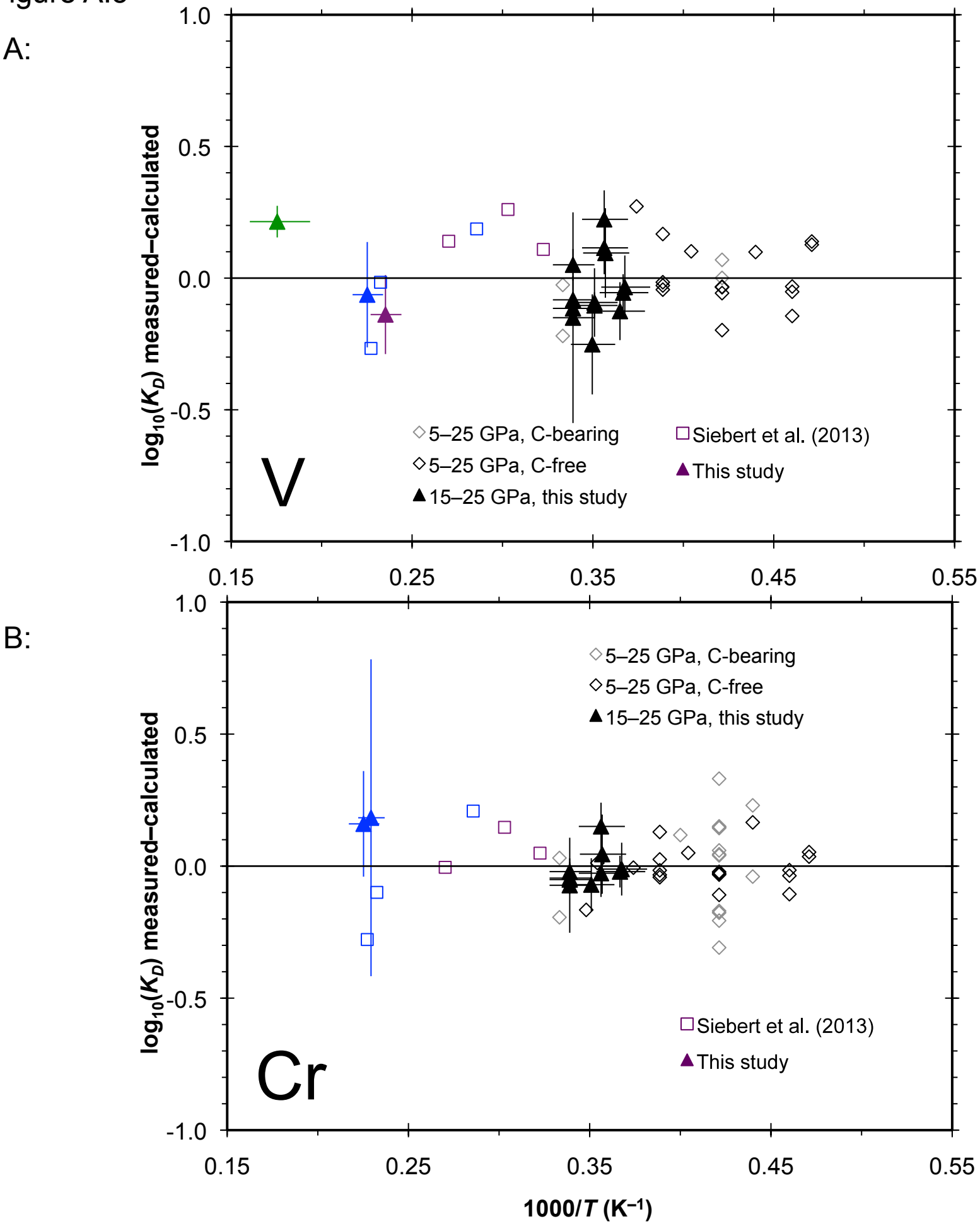
A:
1.0
0.5
0.0
-0.5
-1.0
0.15
0.25
0.35
0.45
0.55
log10(KD) measured–calculated
5–25 GPa, C-bearing
5–25 GPa, C-free
15–25 GPa, this study
Siebert et al. (2013)
This study
V
B:
1.0
0.5
0.0
-0.5
-1.0
0.15
0.25
0.35
0.45
0.55
log10(KD) measured–calculated
5–25 GPa, C-bearing
5–25 GPa, C-free
15–25 GPa, this study
Siebert et al. (2013)
This study
Cr
1000/T (K−1)

Figure A.6

A:

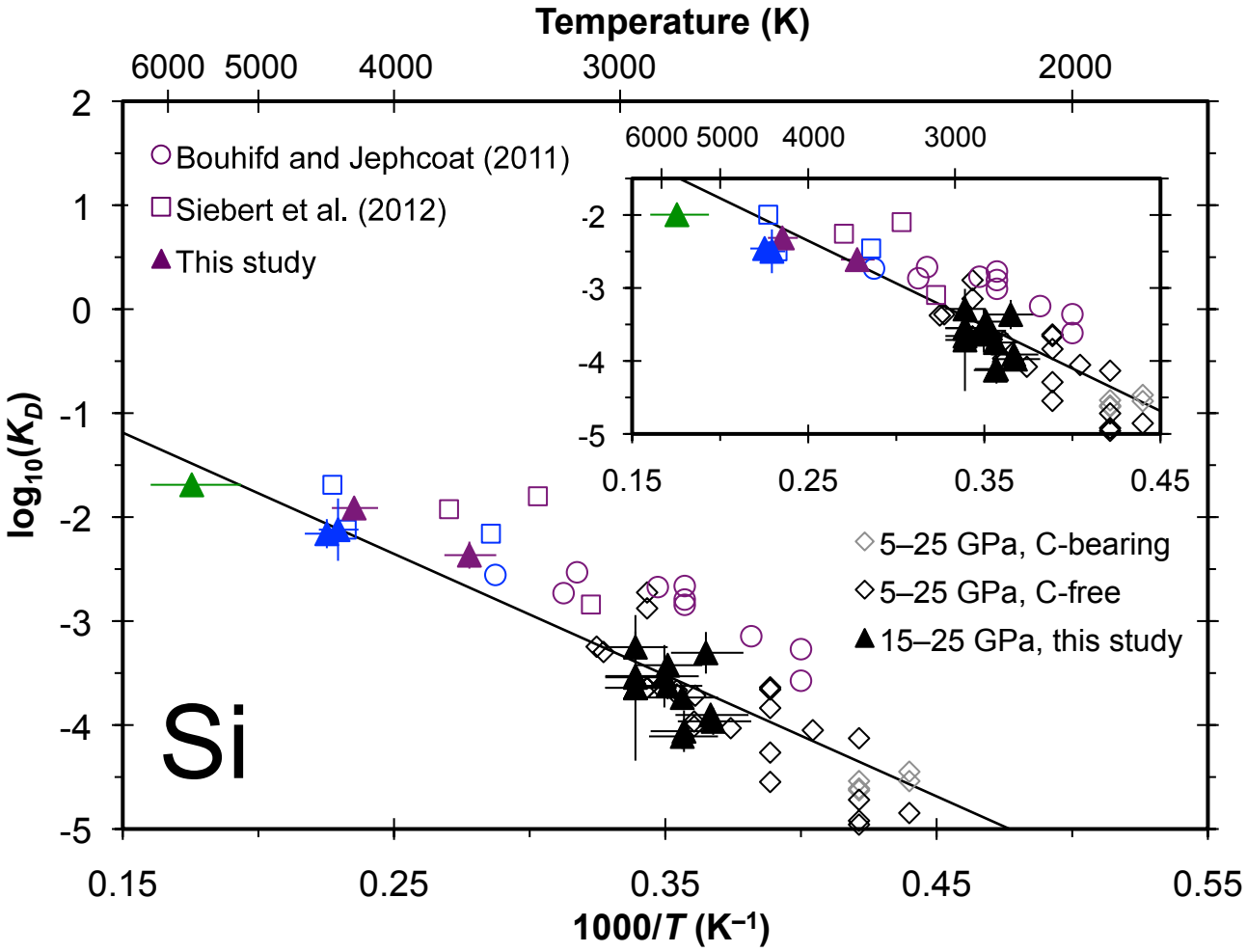
Temperature (K)
6000 5000 4000 3000 2000
Bouhifd and Jephcoat (2011)
Siebert et al. (2012)
This study
5–25 GPa, C-bearing
5–25 GPa, C-free
15–25 GPa, this study
Si
log10(KD)
1000/T (K−1)
0.15 0.25 0.35 0.45 0.55

B:

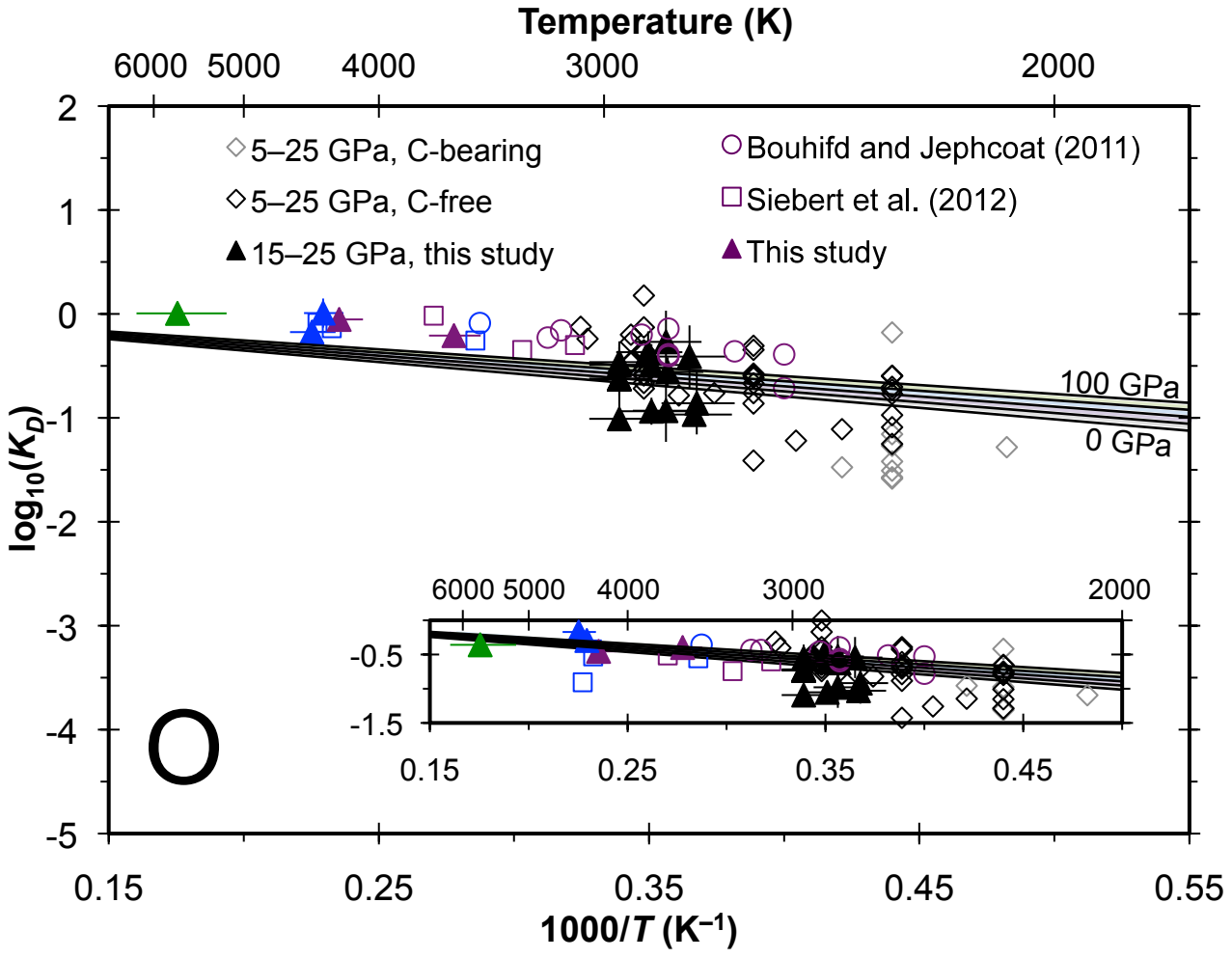
Temperature (K)
6000 5000 4000 3000 2000
5–25 GPa, C-bearing
5–25 GPa, C-free
15–25 GPa, this study
Bouhifd and Jephcoat (2011)
Siebert et al. (2012)
This study
100 GPa
0 GPa
O
log10(KD)
1000/T (K−1)
0.15 0.25 0.35 0.45 0.55